

See discussions, stats, and author profiles for this publication at: <https://www.researchgate.net/publication/264390988>

Pendant Acid–Base Groups in Molecular Catalysts: H–Bond Promoters or Proton Relays? Mechanisms of the Conversion of CO₂ to CO by Electrogenerated Iron(0)Porphyrins Bearing Preposit...

ARTICLE *in* JOURNAL OF THE AMERICAN CHEMICAL SOCIETY · JULY 2014

Impact Factor: 12.11 · DOI: 10.1021/ja506193v · Source: PubMed

CITATIONS

19

READS

160

4 AUTHORS, INCLUDING:



Cyrille Costentin

Paris Diderot University

104 PUBLICATIONS 2,350 CITATIONS

[SEE PROFILE](#)



Marc Robert

Paris Diderot University

114 PUBLICATIONS 2,797 CITATIONS

[SEE PROFILE](#)

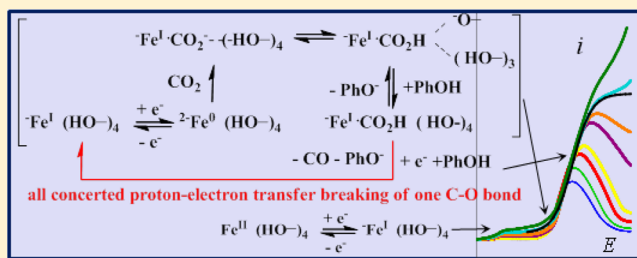
Pendant Acid–Base Groups in Molecular Catalysts: H-Bond Promoters or Proton Relays? Mechanisms of the Conversion of CO₂ to CO by Electrogenerated Iron(0)Porphyrins Bearing Prepositioned Phenol Functionalities

Cyrille Costentin,* Guillaume Passard, Marc Robert, and Jean-Michel Savéant*

Université Paris Diderot, Sorbonne Paris Cité, Laboratoire d'Electrochimie Moléculaire, Unité Mixte de Recherche Université - CNRS No 7591, Bâtiment Lavoisier, 15 rue Jean de Baïf, 75205 Paris Cedex 13, France

Supporting Information

ABSTRACT: Two derivatives of iron tetraphenylporphyrin bearing prepositioned phenolic functionalities on two of the opposed phenyl groups prove to be remarkable catalysts for the reduction of CO₂ to CO when generated electrochemically at the Fe⁰ oxidation state. In one case, the same substituents are present on the two other phenyls, whereas in the other the two other phenyls are perfluorinated. They are taken as examples of the possible role of pendant acid–base groups in molecular catalysis. The prepositioned phenol groups incorporated into the catalyst molecule induce strong stabilization of the initial Fe⁰CO₂ adduct through H-bonding, confirmed by DFT calculations. This positive factor is partly counterbalanced by the necessity, resulting from the same stabilization, to inject an additional electron to trigger catalysis. Thanks to the preprotonation of the initial Fe⁰CO₂ adduct, the potential required for this second electron transfer is not very distant from the potential at which the adduct is generated by addition of CO₂ to the Fe⁰ complex. The protonation step involves an internal phenolic group and the reprotonation of the phenoxide ion thus generated by added phenol. The prepositioned phenol groups thus play both the role of H-bonding stabilizers and high-concentration proton donors. They play the same role in the second electron transfer step which closes the catalytic loop concertedly with the breaking of one of the two C–O bonds of CO₂ and with proton transfer. It is also remarkable that reprotonation by added phenol is concerted with the three other events.



INTRODUCTION

A common law in molecular electrochemistry is that reductions are often accompanied by the loss of a base or the gain of an acid and vice versa for oxidations. In the ubiquitous case where Brønsted acid–base couples are involved, we enter into the realm of proton coupled electron transfers (PCET). This state of affairs transpires in the availability of myriads of Pourbaix diagrams, relating the apparent standard potential of the reactants-to-products couple to the pH. This is not only true for direct electrochemistry but also when the direct electrochemical reaction faces such activation barriers requiring recourse to catalysis. These observations particularly apply to the activation of small molecules addressing the resolution of modern energy challenges.^{1–4} In this connection, Figure 1 recalls the Pourbaix diagrams for the oxidation of water and reduction of dioxygen (a) and reduction of carbon dioxide (b), from ref 5 with permission of the American Chemical Society.

In such cases, as, e.g., in the reduction of CO₂ to CO, catalyzed by electrogenerated iron(0)porphyrin (Scheme 1), the kinetic consequences are that addition of a proton donor, such as phenol, to the solution considerably boosts catalysis.⁶ The next thought was to install phenolic functionalities onto the catalyst molecule itself in such positions as in the molecule designated by CAT (Chart 1) that it would be equivalent to

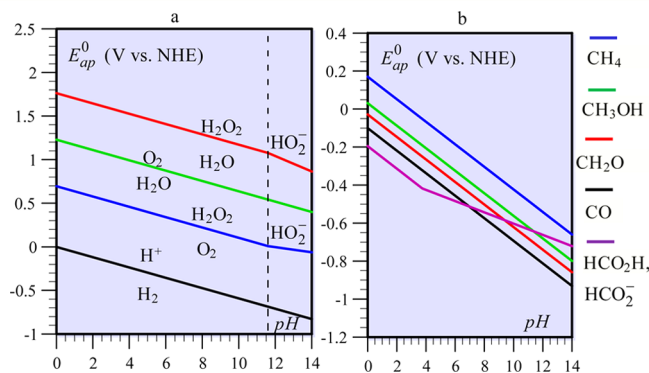


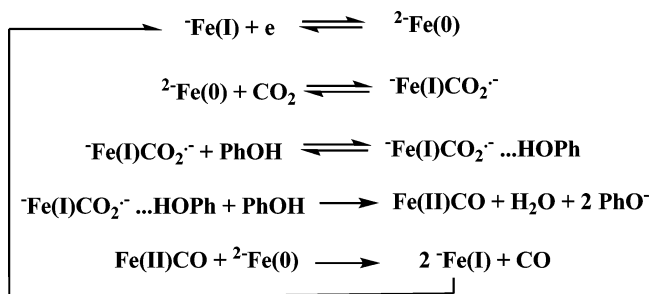
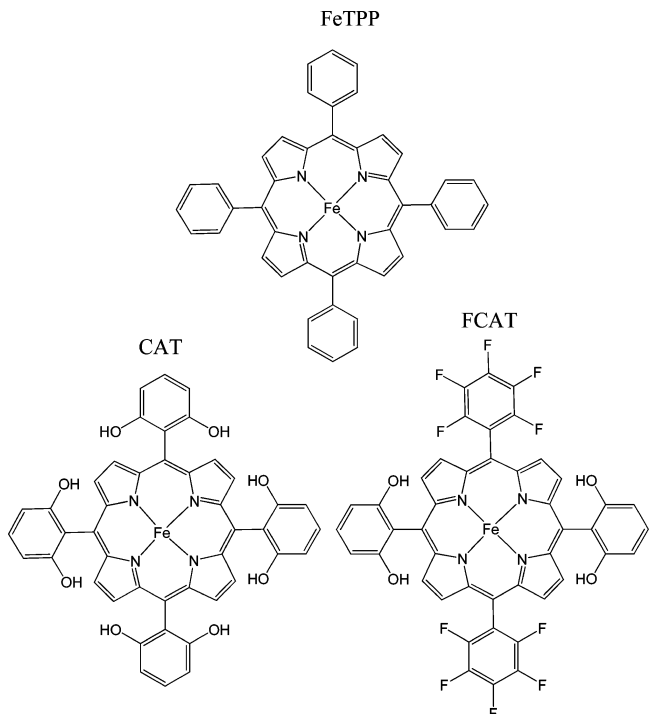
Figure 1. Pourbaix diagrams for the oxidation of water and reduction of dioxygen (a) and reduction of carbon dioxide (b), from ref 5 with permission of the American Chemical Society.

introducing a very large concentration of phenol in the solution without the drawback that its direct reduction could blur the

Received: June 26, 2014

Published: July 30, 2014

Scheme 1

Chart 1⁸

catalytic reaction. A very large catalytic current was indeed observed, as recalled in Figure 2.⁷

The role of the local prepositioned acidic functionalities in the molecule was rationalized by reference to the role of the same acid in solution in boosting catalysis of the CO_2 -to-CO conversion by electrogenerated iron(0)TPP (Chart 1),⁶ in the framework of the reaction scheme depicted in Scheme 1, in which phenol is deemed to act essentially as a proton donor. It was estimated that the presence of the eight phenolic protons in CAT (Chart 1) was equivalent to a 150 M solution.⁷

A more precise investigation of the catalytic characteristics of CAT revealed that the main role of the prepositioned phenolic protons is an H bonding stabilization of the primary CO_2 adduct following the generation of iron(0), which now requires the uptake of an additional electron for catalysis to start. This investigation went in fact through a detour consisting of the study of the catalytic properties of a somewhat different molecule, FCAT, in which four ortho, ortho' phenolic groups are still present on two of the phenyl groups of TPP, while the two others are perfluorinated (Chart 1). The presence of the fluoro groups helped, by means of their electron-withdrawing inductive effect, separating the formation of iron(0) and its CO_2 adduct from its further reduction, which triggers catalysis.

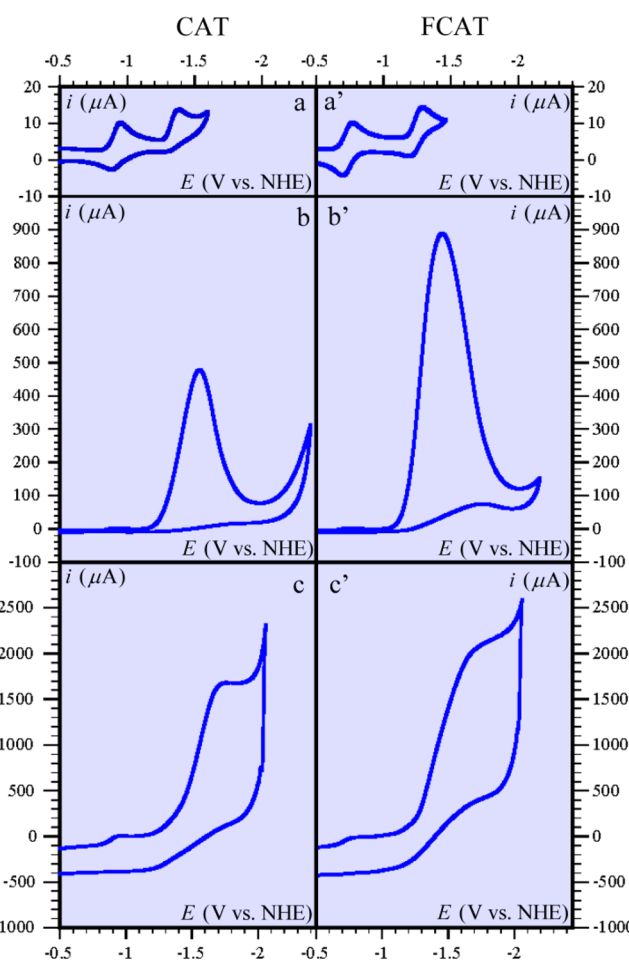


Figure 2. Cyclic voltammetry of 1 mM CAT (a) and FCAT (a') in neat DMF + 0.1 M $n\text{-Bu}_4\text{NPF}_6$ at 0.1 V/s. The same (b, c) and (b', c') in the presence of 0.23 M CO_2 and of 3 M PhOH at 0.1 (b, b') and 20 V/s (c, c').

Deciphering the exact role of the prepositioned phenolic groups in the catalytic mechanism thus required going back and forth between the behaviors of the two molecules, using mostly cyclic voltammetry as a diagnostic tool. Although experiments were the primary source of mechanism determination, quantum chemical calculations helped in confirming assumptions made in the course of data analysis by an investigation of the H-bonding situation in CAT and FCAT.

Determining the respective roles of H-bonding and proton transfer in the two systems investigated here may serve as a model in other catalytic reactions involving other catalyst molecules bearing prepositioned internal acid-base functionalities. Examples of such systems may already be found in the literature concerning catalytic reduction of dioxygen by porphyrins bearing carboxylic acid functionalities⁹ and of hydrogen production and oxidation using nickel-based¹⁰ or cobalt-based molecular catalysts bearing proton relays.¹¹

RESULTS AND DISCUSSION

The investigation of both catalysts was carried out in the presence of a relatively high concentration of phenol in the solution (>0.1 M) so as to avoid the *in situ* formation of persistent deprotonated forms of the catalyst.

Figure 2 shows that FCAT gives rise to a very high catalytic current, even bigger than the catalytic current of CAT. As

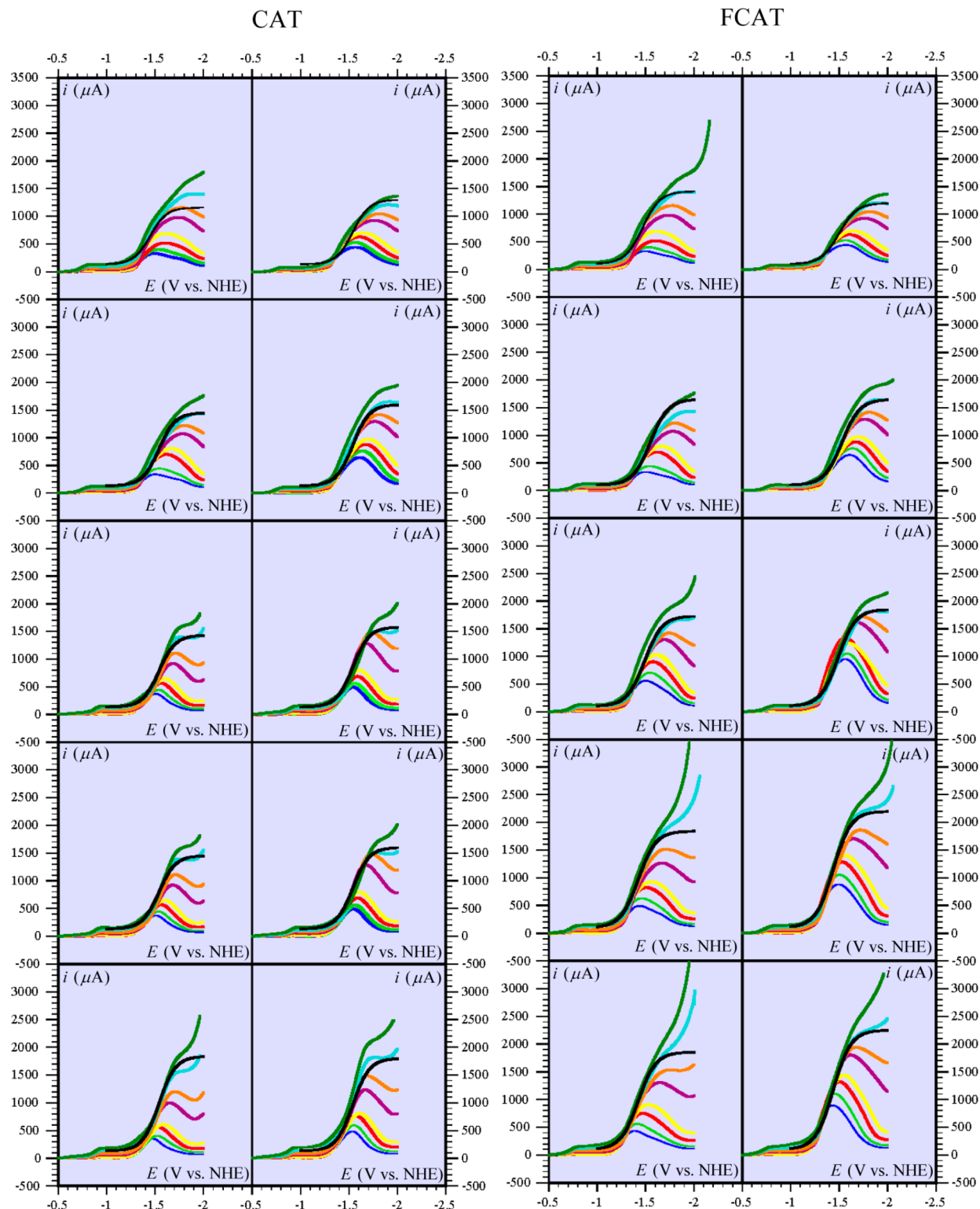


Figure 3. Cyclic voltammetry of 1 mM CAT (left double column) and FCAT (right double column) in DMF + 0.1 M $n\text{-Bu}_4\text{NPF}_6$ in the presence of 0.046 (left) and 0.23 (right) M CO_2 and from top to bottom: 0.3, 0.5, 1, 2, and 3 M PhOH as a function of the scan rate (V/s): 0.1 (blue), 0.2 (light green), 0.5 (red), 1 (yellow), 5 (magenta), 10 (orange), 20 (cyan), and 30 (dark green). In black, simulation of the catalytic current using the parameter values given in Table 1 and Figure 9.

reported in detail elsewhere,¹² preparative-scale electrolysis with FCAT as a catalyst leads to CO in nearly quantitative yield, as observed previously with CAT.⁷

Cyclic Voltammetric Responses of CAT and FCAT in the Presence of CO_2 and PhOH. Figure 3 provides the entire

set of cyclic voltammetric responses obtained at two concentrations of CO_2 , 0.046 and 0.23 M, as a function of the addition of phenol, between 0.3 and 3 M, and of the scan rate (from 0.1 to 30 V/s). Although the two iron porphyrins were introduced in the solution as the Fe^{III} complex, the CV

scan in Figure 3 encompasses only the $\text{Fe}^{\text{II}}/\text{Fe}^{\text{I}}$ and $\text{Fe}^{\text{I}}/\text{Fe}^{\text{0}}$ waves. For clarity, it also depicts only the forward scan of the CV response. It is clear that the catalytic CV responses appearing at the $\text{Fe}^{\text{I}}/\text{Fe}^{\text{0}}$ potential domain are peak-shaped instead of having the canonical S shape expected for fast catalytic processes. However, they come closer to the latter shape upon raising the scan rate. As discussed in detail elsewhere,^{6,7} this behavior points to the interference of side phenomena such as substrate and coreactant consumption and inhibition by products or catalyst deactivation, which decreases with the charge passed during the CV experiment, hence decreasing upon raising the scan rate.

Variations of the CV responses with scan rate and CO_2 and PhOH concentrations are keys to establishing the reaction mechanism. They will be analyzed in detail in the next sections.

Precatalytic Wave. Evidence That Catalysis Requires the Transfer of a Second Electron. A first important remark is that the catalytic wave itself is preceded by a one-electron wave with both catalysts, as seen in Figure 4, even though it is

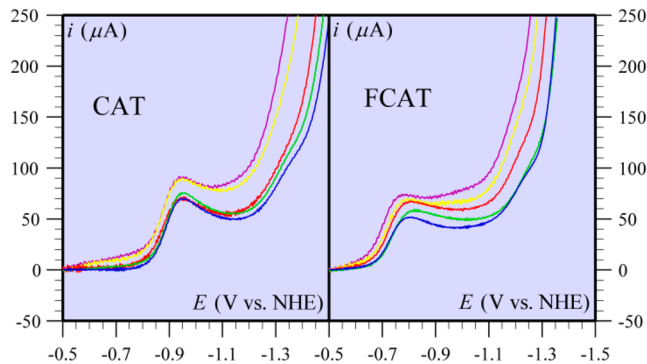
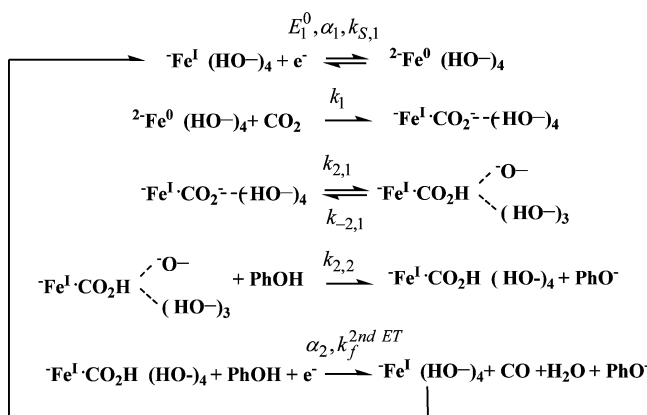


Figure 4. Cyclic voltammetry of 1 mM CAT (left) and FCAT (right) in DMF + 0.1 M $n\text{-Bu}_4\text{NPF}_6$ in the presence of 0.23 M CO_2 at 10 V/s as a function of PhOH concentration (M): 0.3 (blue), 0.5 (light green), 1 (red), 2 (yellow), and 3 (magenta), showing the existence of a prewave, past the first ($\text{Fe}^{\text{II}}/\text{Fe}^{\text{I}}$) wave, and located at the very foot of the catalytic wave.

very close to the catalytic wave. This observation indicates that catalysis requires the uptake of a second electron after the formation of the initial $\text{Fe}^{\text{0}}-\text{CO}_2$ adduct following the reduction of Fe^{I} to Fe^{0} (as in Scheme 2). This is one consequence of the strong stabilization of the $\text{Fe}^{\text{0}}-\text{CO}_2$ adduct (as compared to the case of FeTPP) expected from H-bonding

Scheme 2



involving the hydrogens of the prepositioned phenol groups, which makes the second electron transfer more difficult than the first, unlike the case of FeTPP (see Scheme 2).^{13–15} Quantum chemical calculations (see the Supporting Information) confirm the existence of such H-bonds in the structure of the $\text{Fe}^{\text{0}}-\text{CO}_2$ adduct, as shown in Figure 5. These also show that the main resonant form of the $\text{Fe}^{\text{0}}-\text{CO}_2$ adduct involves a CO_2 anion radical structure, with the second electron being delocalized mainly on the iron but also partly on the porphyrin ring (see details in the Supporting Information).¹⁶

Another consequence of the strong stabilization of the $\text{Fe}^{\text{0}}-\text{CO}_2$ adduct is that the reaction of the Fe^{0} porphyrin with CO_2 may be assumed to be irreversible. There indeed is a large decrease—by ca. 0.4 eV—of the free enthalpy of formation of the $\text{Fe}^{\text{0}}-\text{CO}_2$ adduct when going from FeTPP to CAT (see the Supporting Information). We may then attempt to estimate its rate constant from the characteristics of the prewave as resulting from an “EC” reaction scheme,¹⁷ in which the E-step is the passage from the Fe^{I} to the Fe^{0} complex and the C-step is the irreversible formation of the $\text{Fe}^{\text{0}}-\text{CO}_2$ adduct. This is a difficult venture owing to the overlapping of the prewave and the large catalytic wave, which increases with phenol concentration as the catalytic wave shifts toward positive potentials for reasons that will be developed later on. The situation is somewhat more favorable with FCAT than with CAT, since the potential separation between the two waves is a little larger. Analysis of this EC wave requires measuring the characteristics of the $\text{Fe}^{\text{I}}/\text{Fe}^{\text{0}}$ electron transfer. These were derived from an analysis of the $\text{Fe}^{\text{I}}/\text{Fe}^{\text{0}}$ waves in the absence of CO_2 and PhOH (second waves in the top diagrams of Figure 2). Upon raising the scan rate, they rapidly become chemically reversible.^{18a} The standard potential and standard rate constant are then simply derived from the cathodic and anodic peak potentials and their variations with the scan rate,^{18b} leading to the values reported in Table 1. As seen in Figure 6 (top right), at 0.1 V/s, increasing the CO_2 concentration results in a positive shift of the wave reflecting the kinetic effect of the follow-up reaction (C), i.e., the irreversible formation of the $\text{Fe}^{\text{0}}-\text{CO}_2$ adduct.^{17,18c} As expected, this effect tends to disappear upon raising the scan rate (Figure 6, bottom right), the process being then kinetically controlled by the forward electron transfer step.^{17,18c} Simulation¹⁹ of the experimental data according to this EC reaction scheme led to the values reported in Table 1. In the case of CAT, we were led to use as minimum value of the scan rate $v = 1$ V/s instead of 0.1 V/s for FCAT in order to increase the prewave sufficiently as compared to the catalytic wave (the prewave is expected to grow as $v^{1/2}$, whereas the catalytic wave is expected to be independent of v , at least at the foot of the latter, where the side phenomena are not too prevalent). Under these conditions (left, Figure 6), the dependence toward CO_2 concentration is hardly detectable at 1 V/s and completely disappears, as expected, at 10 V/s. A precise value of k_1 cannot then be obtained, but it may be estimated that it is larger than $5 \times 10^6 \text{ M}^{-1} \text{ s}^{-1}$ (the value used for the simulation in the left of Figure 6 was indeed $5 \times 10^6 \text{ M}^{-1} \text{ s}^{-1}$; for the other parameters, see Table 1).

Object and Characteristics of the Second Electron Transfer. Rate and Mechanism of Protonation of the Initial $\text{Fe}^{\text{0}}-\text{CO}_2$ Adduct. The very existence of a prewave in front of the catalytic wave indicates that the input of a second electron occurs at a potential negative to the potential where the adduct is formed. It seems however quite unlikely that the injection of this second electron into the doubly negatively

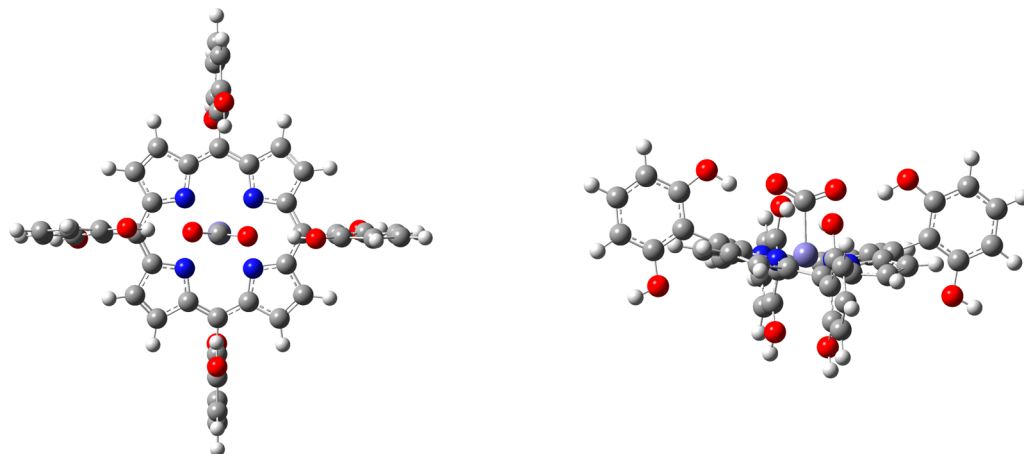


Figure 5. Top (left) and lateral (right) views of the optimized $\text{Fe}^0\text{-CO}_2$ adduct in the case of CAT. Gray, carbon; white, hydrogen; red, oxygen; blue, nitrogen; light purple, iron. See the Supporting Information for details.

Table 1. Thermodynamic and Kinetic Characteristics of the Reactions in Scheme 2

| Reactions ^a | CAT | FCAT |
|---|-------------------|-------------------|
| $\text{Fe}^{\text{I}} + \text{e}^-$ | | |
| E_1^0 (V vs. NHE) | -1.335 | -1.265 |
| α_1 | 0.5 | 0.5 |
| $k_{S,1}$ (cm s^{-1}) | 0.0125 | 0.03 |
| Fe^{I} | | |
| $\text{Fe}^{\text{I}} + \text{CO}_2$ | | |
| k_1 ($\text{M}^{-1}\text{s}^{-1}$) | $> 5 \times 10^6$ | 3×10^5 |
| $\text{Fe}^{\text{I}}\text{-CO}_2^-$ | | |
| $\text{Fe}^{\text{I}}\text{-CO}_2^- + \text{PhOH}$ | | |
| $(k_{2,1} / k_{-2,1})k_{2,2}$ ($\text{M}^{-1}\text{s}^{-1}$) | - | 2.5×10^4 |
| $k_{2,1}$ (s^{-1}) | 7×10^3 | 3×10^4 |
| $\text{Fe}^{\text{I}}\text{-CO}_2\text{H} + \text{PhO}^-$ | | |
| $\text{Fe}^{\text{I}}\text{-CO}_2\text{H} + \text{PhOH} + \text{e}^-$ | | |
| α_2 | 0.3 | |
| $k_f^{2\text{nd ET}}$ (cm s^{-1}) | See figure 9 | |
| $\text{Fe}^{\text{I}} + \text{CO} + \text{OH}_2 + \text{PhO}^-$ | | |

charged CO_2 adduct could occur at a potential so close from the potential at which this adduct is formed. This is the reason that it is much more likely that the second electron uptake occurs after the adduct has been protonated. Protonation of the adduct follows its irreversible formation from Fe^0 and CO_2 and therefore does not influence the prewave. It will however influence the height of the follow-up catalytic wave according to Scheme 2. Two sources are available to protonate the $\text{Fe}^0\text{-CO}_2$ adduct, the internal phenol groups and/or the phenol added to the solution. The first of these protonation reactions is expected to be uphill in view of the scarce basicity of the CO_2 anion radical, expectedly reinforced by H-bonding stabilization by the other internal phenol groups. This is also the case, albeit to a

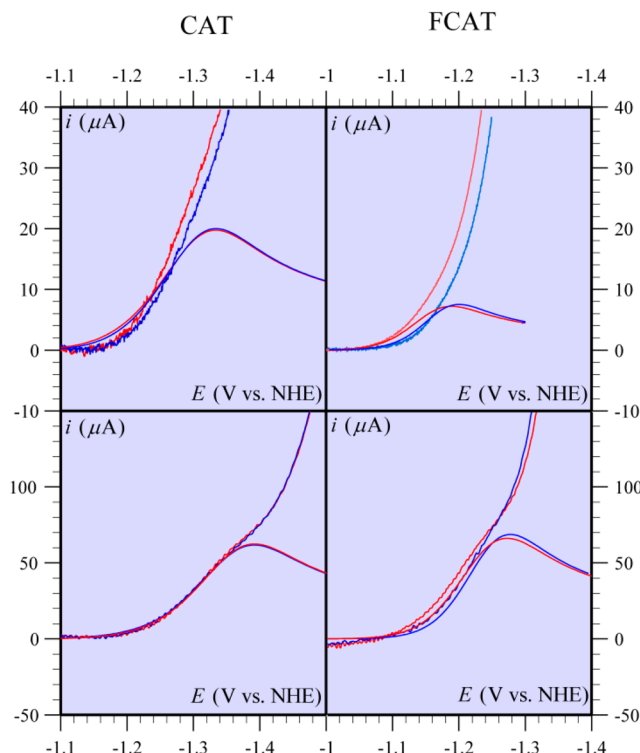


Figure 6. Cyclic voltammetry of 1 mM CAT (left) and FCAT (right) in $\text{DMF} + 0.1 \text{ M } n\text{-Bu}_4\text{NPF}_6$ in the presence of 0.23 (red curves) and 0.046 (blue curves) M CO_2 and 0.3 M PhOH. Scan rate (V/s): top right, 0.1; bottom right, 10; top left, 1; bottom left, 20. Prewave and simulation with the parameter values listed in Table 1. The tailing current of the $\text{Fe}^{\text{II}}/\text{Fe}^{\text{I}}$ wave at the foot of the prewave has been subtracted so that the latter can serve as the zero for the vertical scale.

lesser extent, for the reprotonation of the internal phenoxide ion by phenol in the solution. However, since the medium is not buffered, the concentration of resulting phenoxide ion in the solution is so small that the reverse reaction may be neglected. Once the initial CO_2 adduct has been protonated, its reduction closes the catalytic loop. The height of the quasi-plateau obtained at a scan rate of 20 V/s (Figure 3) may thus serve to gauge the respective role of the rate of formation of the CO_2 adduct and of the rate of its protonation according to Scheme 2.

As shown in the Supporting Information, the plateau current, i_{pl} , may be expressed as

$$i_{pl} = \frac{2FS\sqrt{D_{cat}}C_{cat}^0\sqrt{k_1[CO_2]}}{1 + \frac{\sqrt{k_1[CO_2]}}{\sqrt{k_{2,ap}}}\left(1 + \frac{k_{2,1}}{k_{-2,1} + k_{2,2}C_{PhOH}^0}\right)} \quad (1)$$

where F is the faraday, S the electrode surface area, and D_{cat} and C_{cat}^0 the diffusion coefficient and the concentration of the catalyst, respectively. The other symbols are defined in Scheme 2.

$$k_{2,ap} = \frac{k_{2,1}k_{2,2}C_{PhOH}^0}{k_{-2,1} + k_{2,2}C_{PhOH}^0} \quad (2)$$

is the apparent protonation rate constant, which may be controlled by the reprotonation of the internal Scheme 2 phenoxide ion with the internal protonation at equilibrium ($k_{2,ap} = (k_{2,1}/k_{-2,1})k_{2,2}C_{PhOH}^0$), or upon increasing the concentration of phenol in solution, by the internal protonation step ($k_{2,ap} = k_{2,1}$).

Assuming that step (2,1) is uphill, $k_{2,1}/(k_{-2,1} + k_{2,2}C_{PhOH}^0) \ll 1$ and eq 1 becomes

$$i_{pl} = \frac{2FS\sqrt{D_{cat}}C_{cat}^0\sqrt{k_1[CO_2]}}{1 + \frac{\sqrt{k_1[CO_2]}}{\sqrt{k_{2,ap}}}\left(1 + \frac{\sqrt{k_{2,ap}}}{\sqrt{k_1[CO_2]}}\right)} \quad (1')$$

The fitting of the experimental plateau current with eqs 1' and 2 is shown in Figure 3. The ensuing variations of $k_{2,ap}$ with the phenol concentration in solution are shown in Figure 7.²⁰ Derivation of $k_{2,ap}$ was made possible by the fact that it is smaller than $k_1[CO_2]$ (see eq 1').

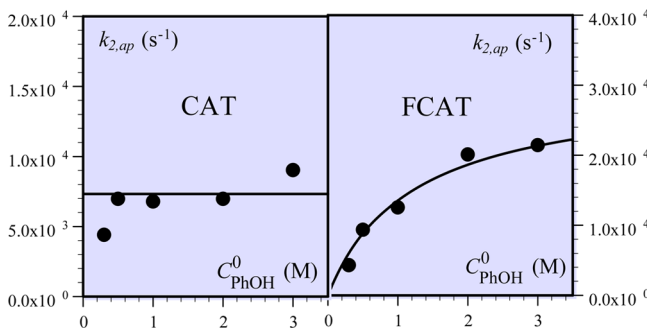


Figure 7. Apparent rate constant of protonation of the Fe^0-CO_2 adduct as a function of the concentration of phenol in the solution.

In the case of FCAT, we observe the transition between the two kinetic regimes, whereas, with CAT, the kinetics is controlled by the forward internal protonation step.²¹ Estimates of the rate constants of the protonation of the Fe^0-CO_2 adduct are given in Table 1.

Evidence That the Second Electron Transfer Is Concerted with a Second Proton Transfer and with the Breaking of One of the C–O Bonds of CO_2 . We may now attempt to fit the whole CV responses in conditions where they are not too far from the canonical S-shape, approximated by the curves obtained at 20 V/s. The slopes of the rising portion of the CV responses point to an irreversible electron transfer process with a transfer coefficient definitely smaller

than 0.5, i.e., to the following equation (see the Supporting Information):

$$i = \frac{i_{pl}}{1 + \exp\left[\alpha_2 \frac{F}{RT}(E - E_{1/2})\right]} \quad (3)$$

with

$$E_{1/2} = \frac{RT \ln 10}{\alpha_2 F} \log k_f^{2nd ET} - \frac{RT \ln 10}{\alpha_2 F} \log \left(\frac{i_{pl}}{2FSC_{cat}^0} \right) \quad (4)$$

where $k_f^{2nd ET} = k_{S,2} \exp(\alpha_2 FE_2^0/RT)$ is the expression of the forward electron transfer rate constant. Indeed, owing to the total irreversibility of this reaction, its standard potential and standard rate constant cannot be gauged separately (note that the value of $k_f^{2nd ET}$ depends on the reference electrode, here NHE). A satisfactory fit of the experimental data with eqs 3 and 4 is obtained as shown in Figure 3 for a value of the transfer coefficient of 0.3 for both catalysts.

The small value of the transfer coefficient is a clear indication that electron transfer in concerted with the breaking of a bond linking two heavy atoms,²² the carbon atom and one of the oxygen atoms of CO_2 , in the present case as pictured in the last line of Scheme 2. Although phenol in solution certainly partakes in the overall step, it is not necessarily engaged in the rate-determining step, which might rather involve one of the internal phenol groups, in a similar way as already discussed in the protonation of the Fe^0CO_2 adduct. In this connection, a better estimation of the forward electron transfer rate constant, $k_f^{2nd ET}$, and particularly of its dependence from the concentration of phenol in solution, is obtained by a linear analysis at the foot of the CV responses according to

$$\log i = \log i_{pl} - \alpha_2 \frac{F}{RT \ln 10} (E - E_{1/2})$$

i.e., taking into account eq 4:

$$\log i = \log k_f^{2nd ET} + \log(2FSC_{cat}^0) - \frac{\alpha_2 F}{RT \ln 10} E \quad (5)$$

The ensuing $0.3 \times F/RT \ln 10$ -slope straight lines represented in Figure 8 were derived from averaging the tangents to the traces obtained at four scan rates—5, 10, 20, and 30 V/s (where the CV responses are not too far from the canonical S-shape)—for a series of phenol concentrations. Rather than extrapolating the straight lines to $E = 0$ V vs NHE, a better precision is reached when remaining within the potential range where the trace was recorded. We thus used the values of the potential where the straight line crosses a horizontal axis defined by a value of the current situated 10^{-4} A above the height of the prewave. Then,

$$\log k_f^{2nd ET} = \frac{\alpha_2 F}{RT \ln 10} E_{(i=10^{-4}A)} + \log(10^{-4} A) - \log(2FSC_{cat}^0)$$

The variations of $E_{(i=10^{-4}A)}$ and $\log k_f^{2nd ET}$ with the concentration of phenol in the solution are shown in Figure 9. At the lower end of the phenol concentration range, the forward rate constant of the second electron transfer is independent of phenol pointing to the involvement of one of the internal phenol groups in the C–O bond breaking process concerted with electron and proton transfers. This is actually expected, since the local concentration of internal phenol

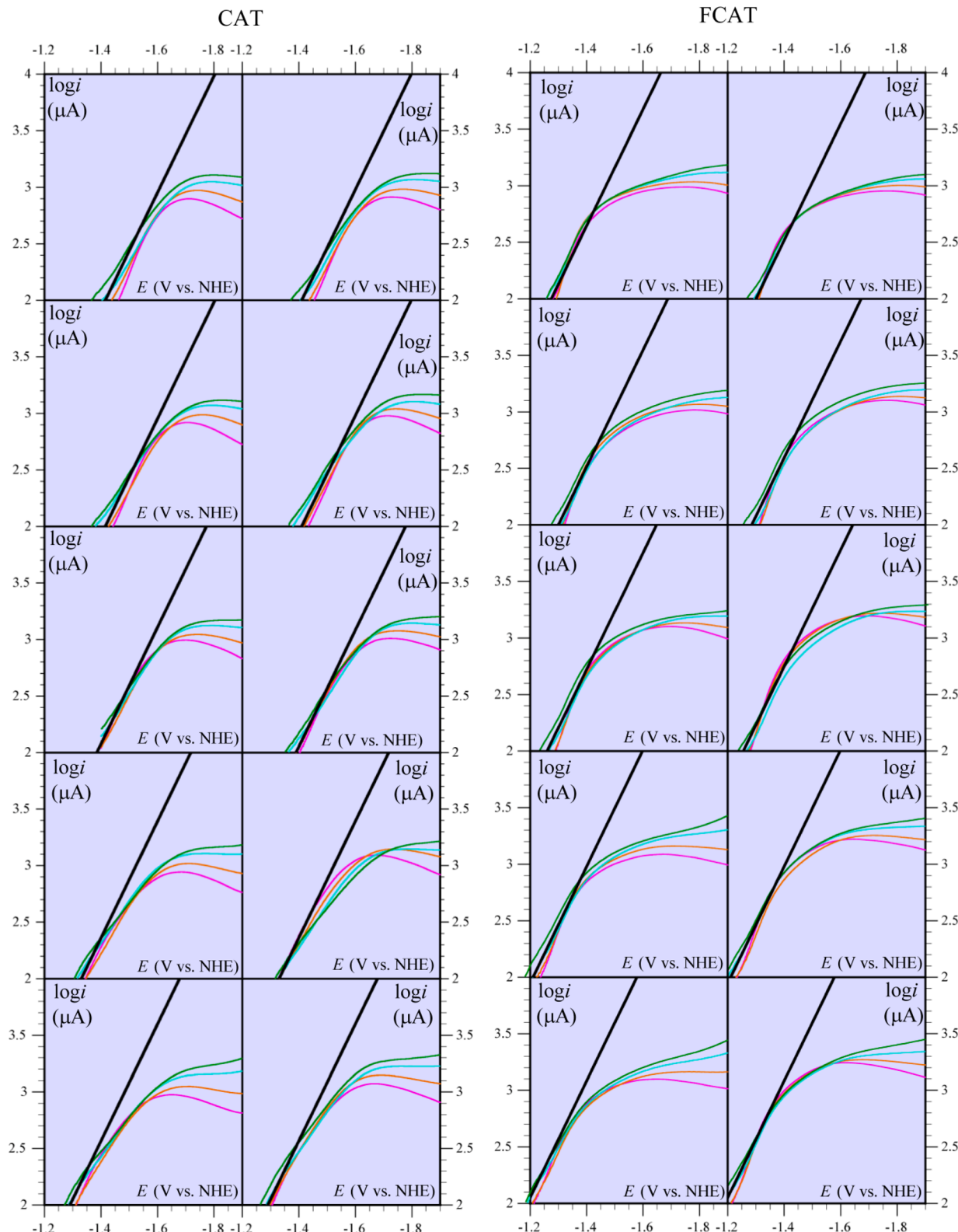


Figure 8. Foot-of-the-wave treatment of some of the data in Figure 3. CAT (left double column) and FCAT (right double column) in the presence of 0.046 (left) and 0.23 (right) M CO_2 and from top to bottom: 0.3, 0.5, 1, 2, and 3 M PhOH as a function of the scan rate ($\text{V}\cdot\text{s}^{-1}$): 5 (magenta), 10 (orange), 20 (cyan), and 30 (dark green). In black, foot-of-the-wave treatment (see text and eqs 4 and 5).

moieties is quite high. Reprotonation of the internal phenoxide ion thus generated by solution phenol would then occur in a second step following the rate-determining bond breaking concerted with electron and internal proton transfer. It is

however noteworthy that the second electron transfer rate constant starts to increase upon reaching high concentrations of solution phenol. We may relate this observation to a situation where reprotonation by solution phenol would be concerted

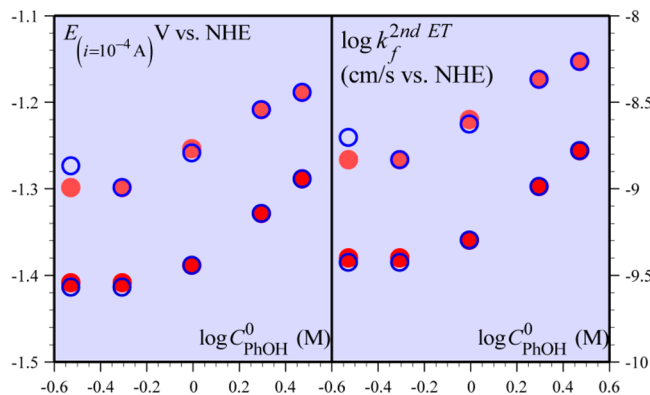


Figure 9. Potential at $i = 10^{-4}$ A (left) and forward rate constant of the second electron transfer (right) as a function of the concentration of phenol in solution. Red dots are for $[CO_2] = 0.23$ M and blue open circles for $[CO_2] = 0.046$ M. The upper series of data points is for FCAT and the lower for CAT. See text for an explanation of the units and the dependence toward the reference electrode.

with the concerted bond breaking electron and internal proton transfer process. As surprising as such all-concerted processes may look at first glance, they are actually well documented in the oxidation of phenols driven by neighboring basic groups through H-bond relays.²³

With all the parameter values in hand (Table 1 and Figure 9), a final check consisted of simulating the expected S-shaped scan-rate-independent catalytic CV responses. As seen in Figure 3, there is a good fit between these simulated curves and the experimental curves obtained for the highest scan rates, when the interference of the side phenomena is minimal.

As shown in the Supporting Information (Figure S1), the H/D isotopic effect on the CV responses is one within experimental uncertainty. The reason for this is presumably that the last three steps in Scheme 2 are expected to be little sensitive to isotope effects in spite that they involve internal phenol groups or added phenol. The third and fourth steps are uphill reactions. The potential variations of the two pK's that determine the equilibrium constant are likely to compensate each other, and the H-to-D variations of the barrierless reverse internal or diffusion-controlled external reactions are not expected to be large. The fifth step, being a strongly downhill electron transfer concerted with proton transfer and breaking of a bond between heavy atoms, is also expected to be little sensitive to isotope effects.²²

CONCLUDING REMARKS

Starting from the remarkable catalytic properties of the two molecules CAT and FCAT, the comparative analysis of their cyclic voltammetry as a function of the scan rate and of the concentrations of CO_2 and added phenol has made it possible to unravel a rather complex mechanism in spite of the adverse occurrence of side phenomena such as substrate consumption, inhibition by products, and deactivation of the catalyst. The presence of prepositioned phenol groups inside the catalyst molecule results in a strong stabilization of the initial Fe^0CO_2 adduct through H-bonding. This positive factor is partly counterbalanced by the necessity, resulting from the same stabilization, to inject an additional electron to trigger catalysis. Thanks to the preprotonation of the initial Fe^0CO_2 adduct, the potential required for this second electron transfer is not very distant from the potential at which the adduct is generated by

addition of CO_2 to the Fe^0 complex. The protonation step involves an internal phenolic group and the reprotoonation of the phenoxide ion thus generated by added phenol. At this stage, it may thus be concluded that the prepositioned phenol groups play both the role of H-bonding stabilizers and high-concentration proton donors. The second electron transfer step required to close the catalytic loop is a reaction in which electron transfer is concerted with the breaking of one of the two C–O bonds of CO_2 and with proton transfer. This is a new case among the few well-characterized examples of these all-concerted reactions endowed with a large driving force owed not only to bond breaking but also to concerted proton transfer, which allows an efficient crossing of the barrier deriving from the cleavage of the bond linking the two heavy atoms. Here too, the prepositioned phenol groups play the role of H-high-concentration proton donors. It is also remarkable that reprotoonation by added phenol may also be concerted with the three other events.

EXPERIMENTAL SECTION

Chemicals. Dimethylformamide (Acros, >99.8%, extra dry over molecular sieves), the supporting electrolyte $n\text{-}NBu_4PF_6$ (Fluka, puriss.), phenol (Alfa-Aesar), and PhOD (Sigma-Aldrich) were used as received. CAT⁷ and FCAT¹² were synthesized as described elsewhere. An Alphagaz Air Liquide mass flow regulator was used for the reduced CO_2 pressure experiments.

Cyclic Voltammetry. The working electrode was a 3 mm diameter glassy carbon (Tokai) disk carefully polished and ultrasonically rinsed in absolute ethanol before use. The counter electrode was a platinum wire. The reference electrode was an aqueous SCE electrode. All experiments were carried out under argon or carbon dioxide (or a mixing of both gases) at 21 °C, the double-wall jacketed cell being thermostated by circulation of water. Cyclic voltammograms were obtained by use of a Metrohm AUTOLAB instrument. Ohmic drop was compensated using the positive feedback compensation implemented in the instrument.

ASSOCIATED CONTENT

S Supporting Information

Proof of eqs 1–5, H/D isotopic effects, and quantum chemical calculations. This material is available free of charge via the Internet at <http://pubs.acs.org>.

AUTHOR INFORMATION

Corresponding Authors

cyrille.costentin@univ-paris-diderot.fr
saveant@univ-paris-diderot.fr

Notes

The authors declare no competing financial interest.

ACKNOWLEDGMENTS

Partial financial support from the Agence Nationale de la Recherche Scientifique (ANR 2010 BLANC 0808) is gratefully acknowledged. Dr. Aurélie Perrier-Pineau (Univ. Paris Diderot, UMR 7086) is gratefully acknowledged for her helpful advice on quantum chemical calculations.

REFERENCES

- (1) Lewis, N. S.; Nocera, D. G. *Proc. Natl. Acad. Sci. U.S.A.* **2006**, *103*, 15729.
- (2) Benson, E. E.; Kubiak, C. P.; Sathrum, A. J.; Smieja, J. M. *Chem. Soc. Rev.* **2009**, *38*, 89.
- (3) Gray, H. B. *Nat. Chem.* **2009**, *1*, 7.
- (4) Artero, V.; Fontecave, M. *Chem. Soc. Rev.* **2013**, *42*, 2338.

- (5) Savéant, J.-M. *Chem. Rev.* **2008**, *108*, 2348.
- (6) (a) Costentin, C.; Drouet, S.; Passard, G.; Robert, M.; Savéant, J.-M. *J. Am. Chem. Soc.* **2013**, *135*, 9023. (b) Costentin, C.; Drouet, S.; Robert, M.; Savéant, J.-M. *J. Am. Chem. Soc.* **2012**, *134*, 11235, 19949.
- (7) Costentin, C.; Drouet, S.; Robert, M.; Savéant, J.-M. *Science* **2012**, *338*, 90.
- (8) In fact, the four phenyl rings are perpendicular to the porphyrin ring in all cases.
- (9) (a) Matson, B. D.; Carver, C. T.; Von Ruden, A.; Yang, J. Y.; Raugei, S.; Mayer, J. M. *Chem. Commun.* **2012**, *48*, 11100. (b) Carver, C. T.; Matson, B. D.; Mayer, J. M. *J. Am. Chem. Soc.* **2012**, *134*, 5444. (c) Samanta, S.; Das, P. K.; Chatterjee, S.; Sengupta, K.; Mondal, B.; Dey, A. *Inorg. Chem.* **2013**, *52*, 12963.
- (10) (a) Wilson, A. D.; Newell, R. H.; McNevin, M. J.; Muckerman, J. T.; Rakowski DuBois, M.; DuBois, D. L. *J. Am. Chem. Soc.* **2005**, *128*, 358. (b) Wilson, A. D.; Newell, R. H.; McNevin, M. J.; Muckerman, J. T.; Rakowski DuBois, M.; DuBois, D. L. *J. Am. Chem. Soc.* **2006**, *128*, 358. (c) Rakowski Dubois, M.; Dubois, D. L. *Acc. Chem. Res.* **2009**, *42*, 1974.
- (11) (a) Roubelakis, M. M.; Bediako, D. K.; Dogutan, D. K.; Nocera, D. G. *Energy Environ. Sci.* **2012**, *5*, 7737. (b) Lee, C. H.; Dogutan, D. K.; Nocera, D. G. *J. Am. Chem. Soc.* **2011**, *133*, 8775.
- (12) Costentin, C.; Passard, G.; Robert, M.; Saveant, J.-M. Submitted for publication.
- (13) This is one of many systems in which catalysis requires the input of a second electron into the adduct formed upon reaction of the substrate with a form of the catalyst resulting from a first electron transfer. See, e.g., refs 14 and 15.
- (14) (a) Lexa, D.; Savéant, J.-M.; Soufflet, J. P. *J. Electroanal. Chem.* **1979**, *100*, 159. (b) Arguello, J. E.; Costentin, C.; Griveau, S.; Savéant, J.-M. *J. Am. Chem. Soc.* **2005**, *127*, 5049. (c) Costentin, C.; Passard, G.; Robert, M.; Savéant, J.-M. *Chem. Sci.* **2013**, *4*, 819.
- (15) Baffert, C.; Artero, V.; Fontecave, M. *Inorg. Chem.* **2007**, *46*, 1817.
- (16) That the main resonant form of the Fe^0CO_2 adduct involves an anion radical structure of CO_2 also emerged from a previous analysis of the mechanism of the catalytic conversion of CO_2 to CO by means of electrogenerated iron(0)TPP in the presence of Brønsted acids.^{6a}
- (17) Savéant, J.-M. *Elements of molecular and biomolecular electrochemistry: an electrochemical approach to electron transfer chemistry*; John Wiley & Sons: Hoboken, NJ, 2006; Chapter 2.
- (18) (a) The slight irreversibility noted at low scan rate presumably results from the catalytic reduction of acidic impurities, including residual water. (b) Chapter 1 in ref 17. (c) Nadjo, L.; Savéant, J.-M. *J. Electroanal. Chem.* **1973**, *48*, 113.
- (19) Using the Digielch software: Rudolph, M. *J. Electroanal. Chem.* **2003**, *543*, 23.
- (20) With FCAT, the rate constant k_1 is known from the analysis of the prewave, thus allowing the derivation of $k_{2,\text{ap}}$ by means of eq 1. In the case of CAT, the analysis of the prewave provides only an upper limit of k_1 . However, this is so large that its exact value does not really matter, since the kinetics at the plateau is then practically controlled by $k_{2,\text{ap}}$.
- (21) Beyond the unavoidable uncertainties on the estimation of the rate constants, it appears that $k_{2,1}^{\text{CAT}} < k_{2,1}^{\text{FCAT}}$ and that $(k_{-2,1}/k_{2,2})^{\text{CAT}} < (k_{-2,1}/k_{2,2})^{\text{FCAT}}$. This may be rationalized by first noting as likely that $k_{2,2}^{\text{CAT}} < k_{2,2}^{\text{FCAT}}$ owing to the larger basicity of the internal phenoxide ion in CAT than that in FCAT. That $k_{2,1}^{\text{CAT}} < k_{2,1}^{\text{FCAT}}$ may then be related to the larger acidity of the internal phenol groups in FCAT as compared to CAT that may overcompensated by the weaker basicity of the $\text{Fe}(0)\text{CO}_2$ adduct in the former case as compared to the latter.
- (22) For a recent theoretical and experimental discussion of this type of reactions, where the breaking of a heavy-atom bond is concerted with electron transfer and proton transfer, see: Costentin, C.; Robert, M.; Savéant, J.-M.; Tard, C. *Acc. Chem. Res.* **2014**, *47*, 271.
- (23) (a) Costentin, C.; Robert, M.; Savéant, J.-M.; Tard, C. *Angew. Chem., Int. Ed.* **2010**, *49*, 3803. (b) Bonin, J.; Costentin, C.; Robert, M.; Savéant, J.-M.; Tard, C. *Acc. Chem. Res.* **2012**, *45*, 372; **2013**, *46*, 1910.